Supplementary Information

Low-Intensity Focused Ultrasound-Assisted Nanocomposite for Advanced Triple Cancer Therapy: Local Chemotherapy, Therapeutic Extracellular Vesicles and Combined Immunotherapy

Mixiao Tan[a], Yuli Chen[b], Yuan Guo[a], Chao Yang[a], Mingzhu Liu[a], Dan Guo[a], Zhigang Wang[a], Yang Cao*[a] and Haitao Ran*[a],

[a] *The Second Affiliated Hospital of Chongqing Medical University & Chongqing Key Laboratory of Ultrasound Molecular Imaging, Chongqing, 400010, China*

[b] *Chongqing Dazu District People's Hospital, Chongqing, 402360, China*

*Corresponding author.

E-mail address: ranhaitao@cqmu.edu.cn (H. Ran), caoyangcqu@163.com (Y. Cao)

Supplementary figures

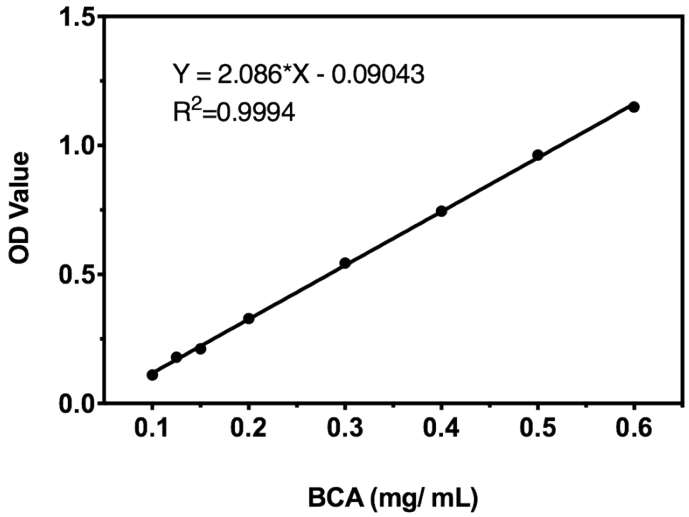

Figure S1. The concentration-absorbance standard curve of bicinchoninic acid (BCA) protein.

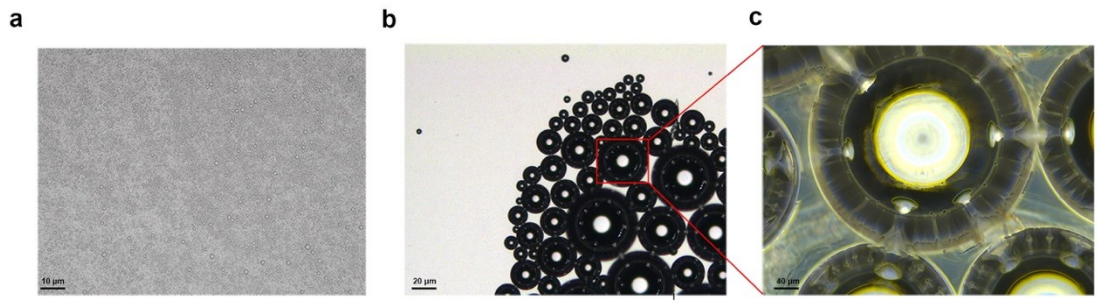

Figure S2. The pH-responsive gas-generating behavior of the CCs-SF/DOX NPs. (a, b) Optical microscopy images of the NPs after incubation in acetate buffer solution at pH 6.5 for 30 min. (c) Enlarged specific structure of the bubbles. In high magnification fields of optical microscopy, when many bubbles gathered together, the contact interface of each bubble generated some specific pore canals, where the number of pore canals was in line with the number of contacted bubbles (b, c). Moreover, due to the negative pressure of the pore canals in larger bubbles, smaller bubbles were drawn to it spontaneously. Gas exchange between smaller bubbles and larger bubbles was achieved through these pore canals, and then these larger bubbles (>micrometer) could be visualized by US.

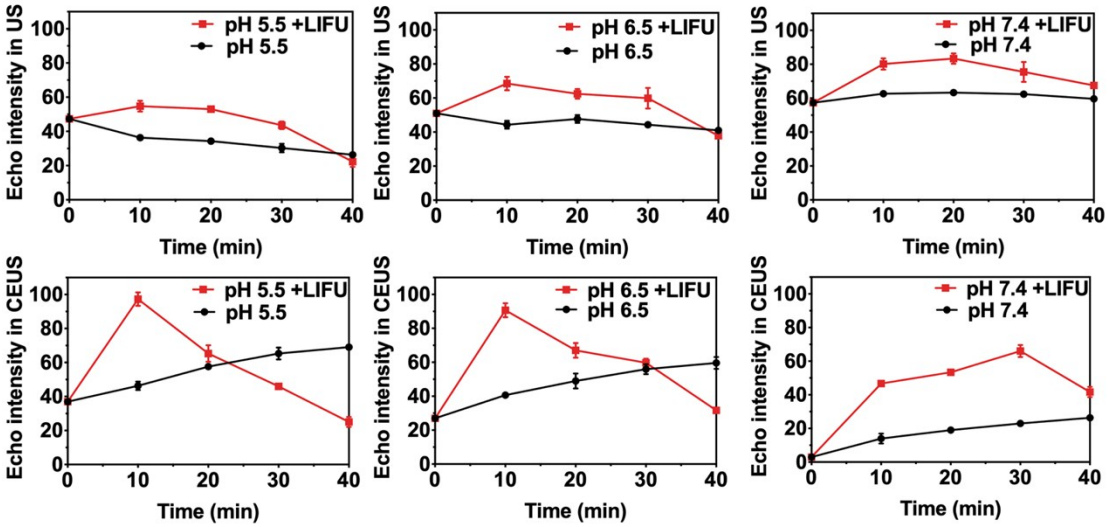

Figure. S3. Quantification of echo intensity (EI) of US and CEUS images obtained at different pH values at 0 min, 10 min, 20 min, 30 min and 40 min respectively.

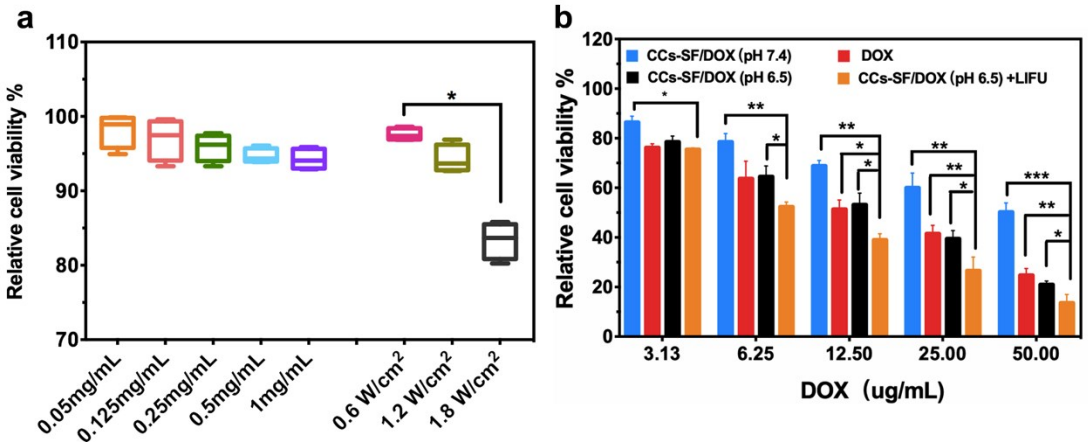

Figure S4. Cytotoxicity assay of CCs-SF, free DOX, CCs-SF/DOX at pH 7.4, CCs-SF/DOX at pH 6.5, CCs-SF/DOX at pH 6.5 plus LIFU incubated with 4T1 cells for 24 h with different concentrations and various LIFU powers (a, b). The results were expressed as the mean ± standard deviation (SD), *P < 0.05, **P < 0.01, or ***P < 0.001.

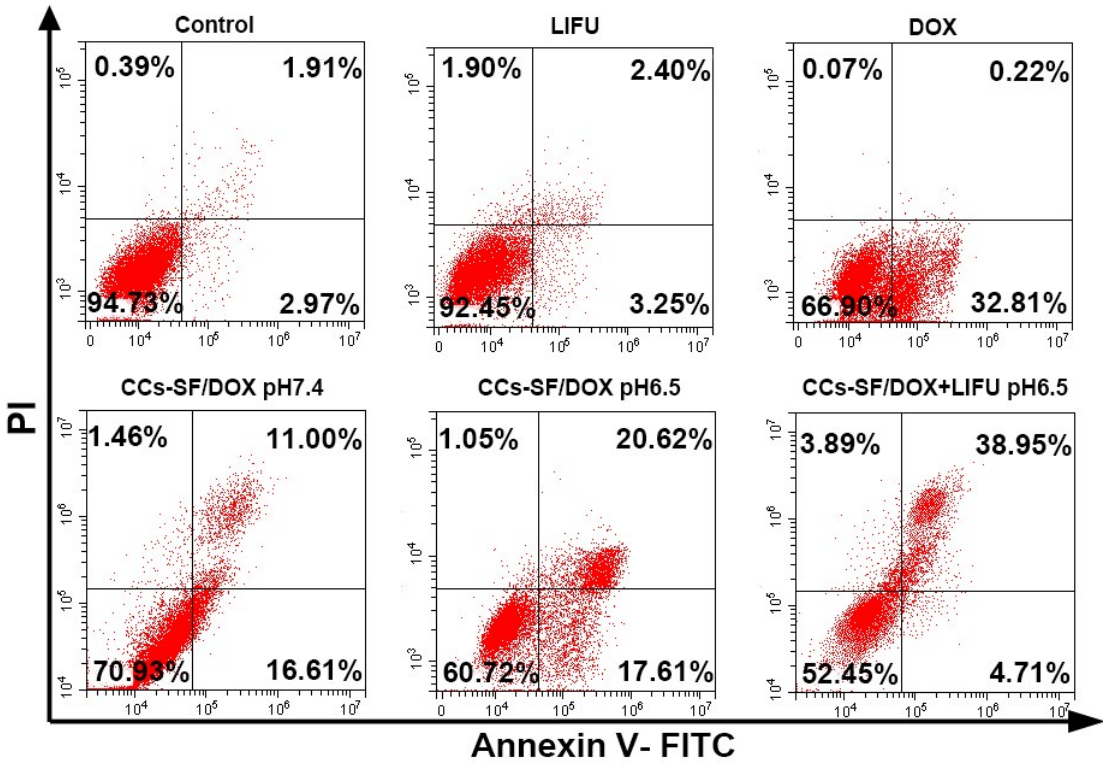

Figure S5. Flow cytometry analysis of 4T1 cell apoptosis induced by different treatments after 8 h using annexin V-FITC/PI staining. Among all the samples, the NPs combined with LIFU at pH 6.5 showed the highest total apoptotic ratio of 43.66% (early apoptotic ratio of 38.95% and late apoptotic ratio of 4.71%) and the lowest viability of 52.45%. Moreover, the group of cells incubated with CCs-SF/DOX at pH 6.5 showed higher cytotoxicity than the group of cells incubated with free DOX and CCs-SF/DOX at pH 7.4.

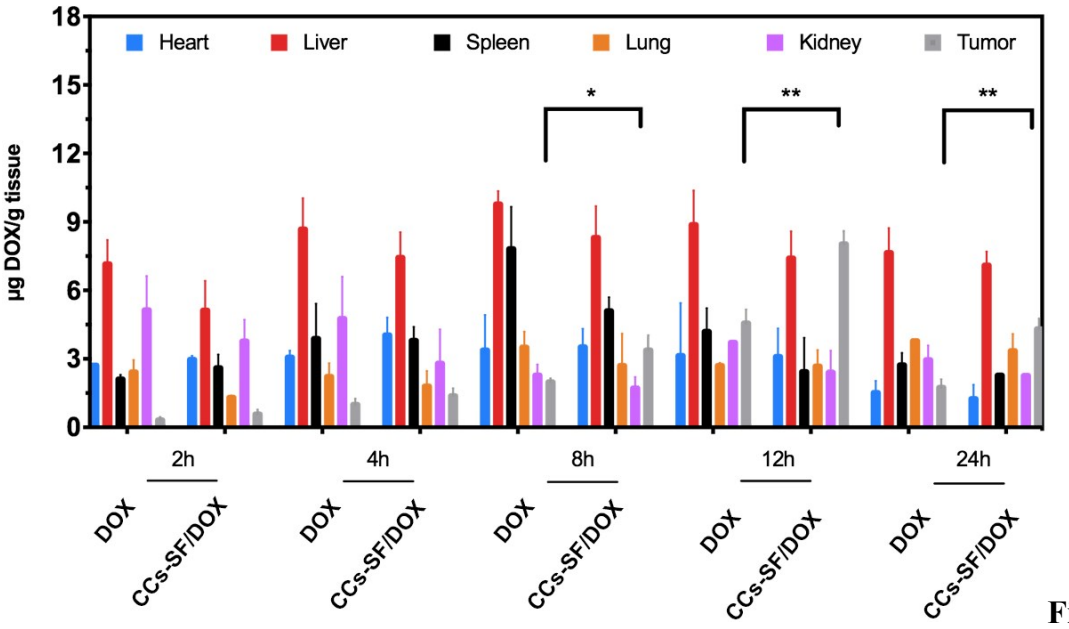

Figure S6. Tissue distribution of total DOX after intravenous administration of CCs-SF/DOX and DOX. Data were expressed as the mean ± standard deviation (n = 4, *P < 0.05, **P < 0.01).

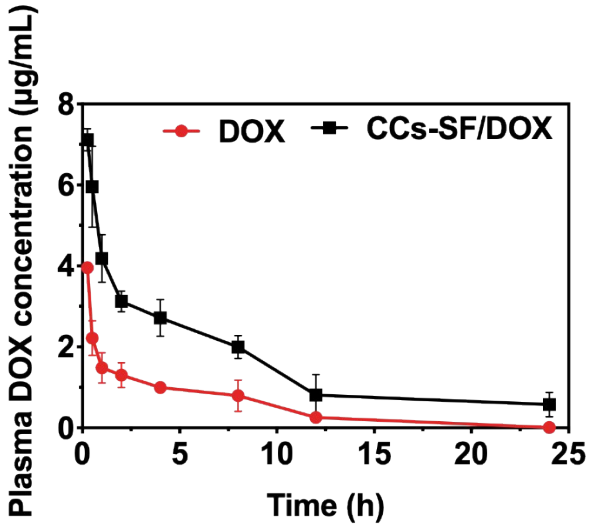

Figure S7. Time-dependent plasma concentration of total DOX after intravenous administration of CCs-SF/DOX and DOX. Data were expressed as the mean ± standard deviation (n = 4).

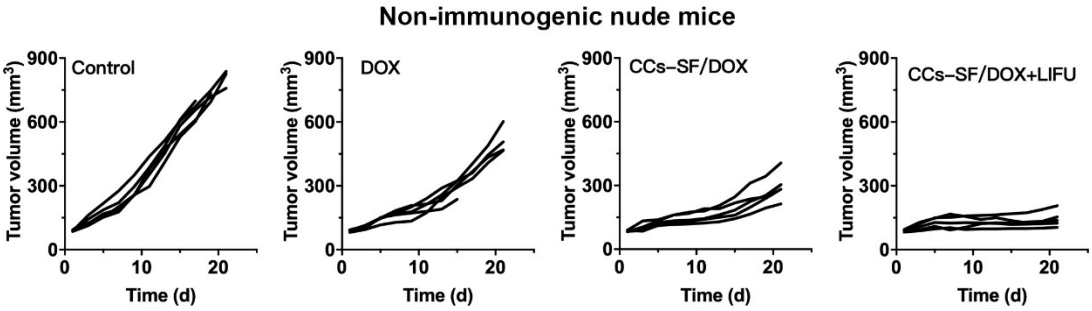

Figure S8. Individual tumor growth kinetics of different groups in non-immunogenicity nude mice.

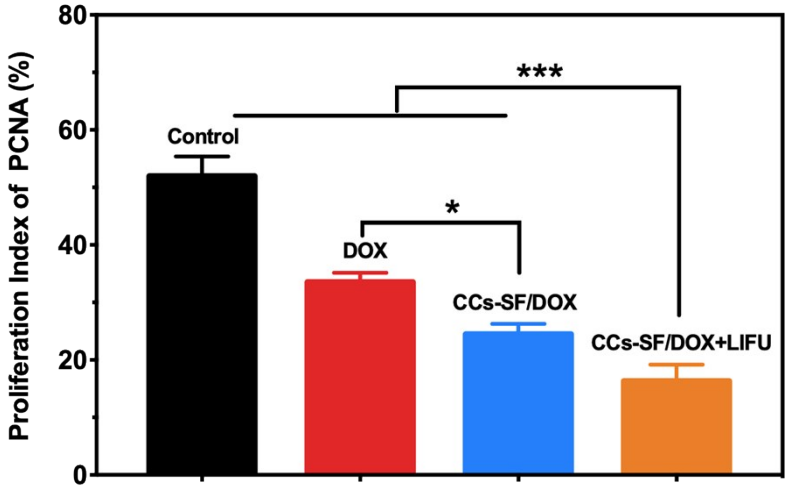

Figure S9. The proliferation index (PI) of PCNA in each group. The data were expressed as the mean ± standard deviation (n = 5, *P < 0.05, **P < 0.01, or ***P < 0.001).

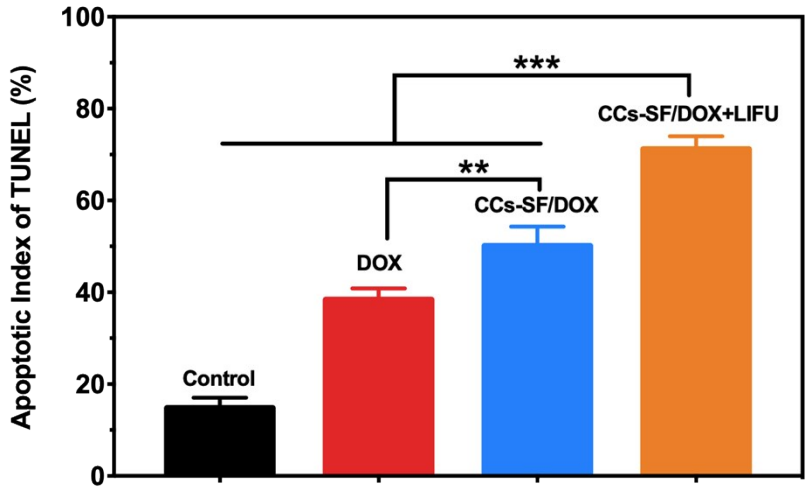

Figure S10. The apoptotic index (AI) of TUNEL in each group. The data were expressed as the mean ± standard deviation (n = 5, *P < 0.05, **P < 0.01, or ***P < 0.001).

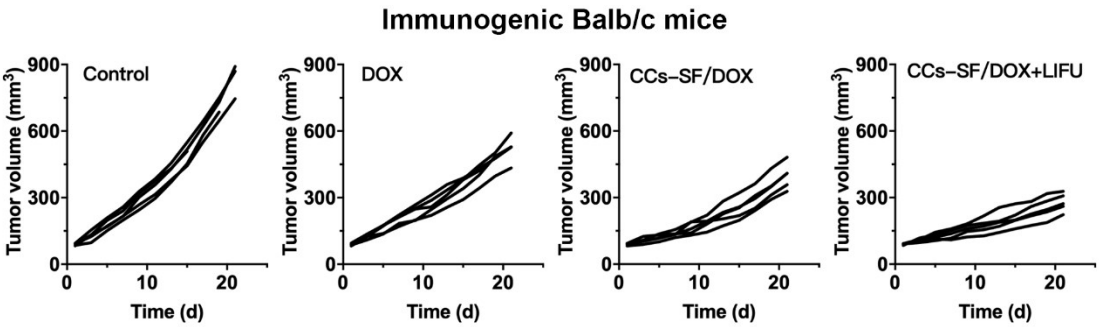

Figure S11. Individual tumor growth kinetics of different groups in immunogenic Balb/c mice.

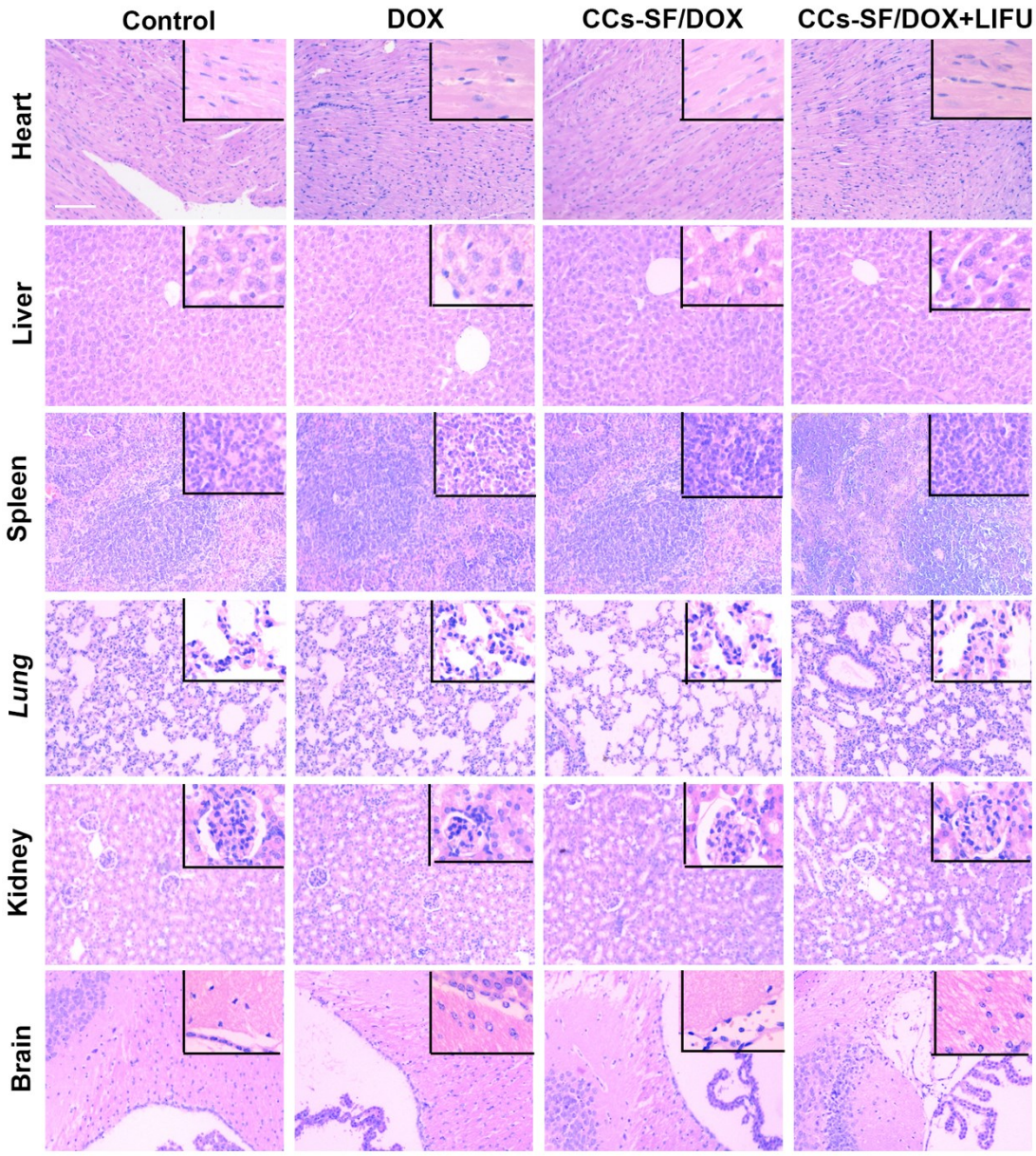

Figure S12. H&E-stained tissue sections of major organs (heart, liver, spleen, lung, kidney and brain) of mice bearing 4T1 tumors after different treatments for 21 days. Magnification was 100× and 400× (inset picture); scale bar is 200 μm.

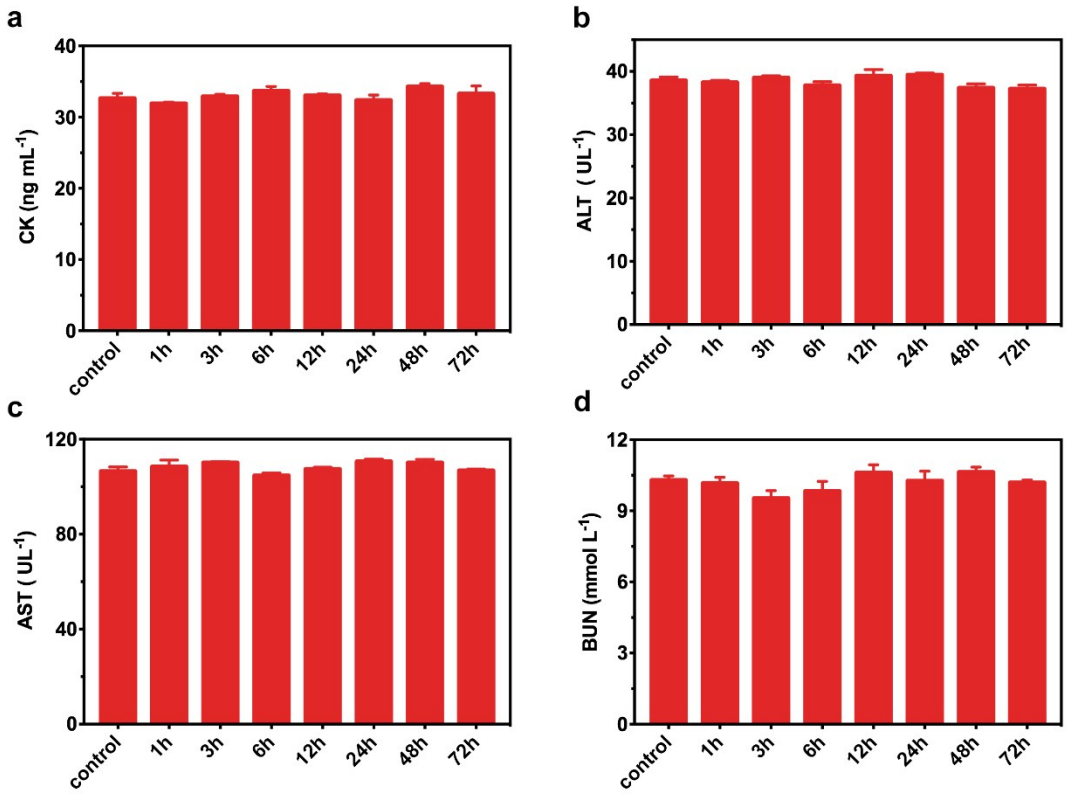

Figure S13. Evaluations of CK, ALT, AST, and BUN by ELISA kits after different intravenously administered of CCs-SF/DOX for 1 h, 3 h, 6 h, 12 h, 24 h, 48 h (n = 4).

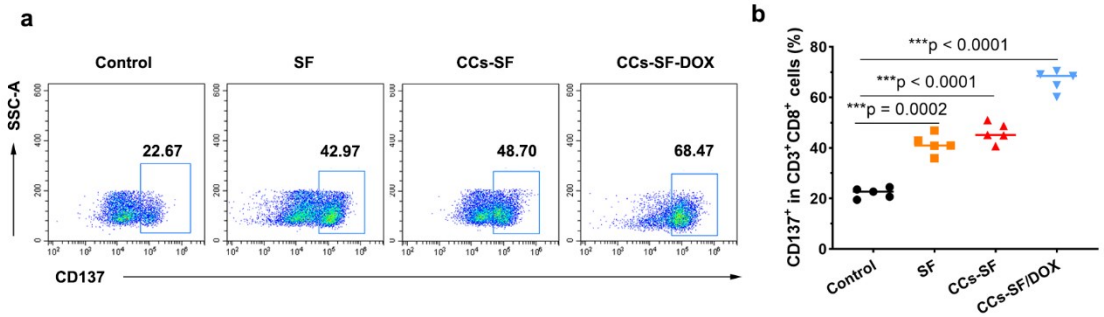

Figure S14. Representative images (a) and the relative quantification of flow cytometric analysis of $CD137^+$ gating on $CD3^+CD8^+$ cells (b). Data were expressed as the mean ± SD (n = 5, *P < 0.05; **P < 0.01; ***P < 0.001).

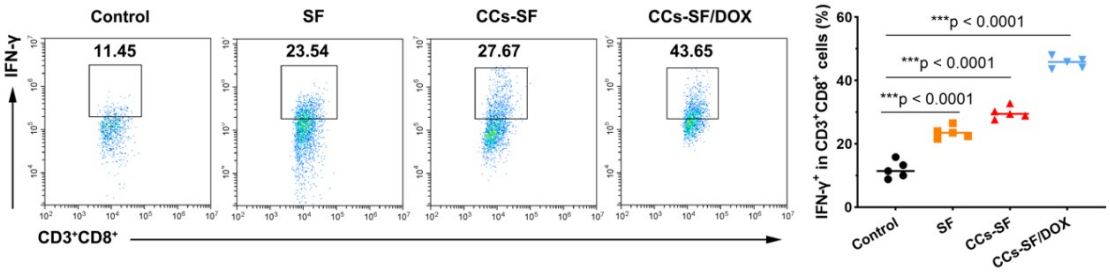

Figure S15. Representative images (a) and the relative quantification of flow cytometric analysis of IFN-γ^+ gating on $CD3^+CD8^+$ cells (b). Data were expressed as the mean ± SD (n = 5, *P < 0.05; **P < 0.01; ***P < 0.001).

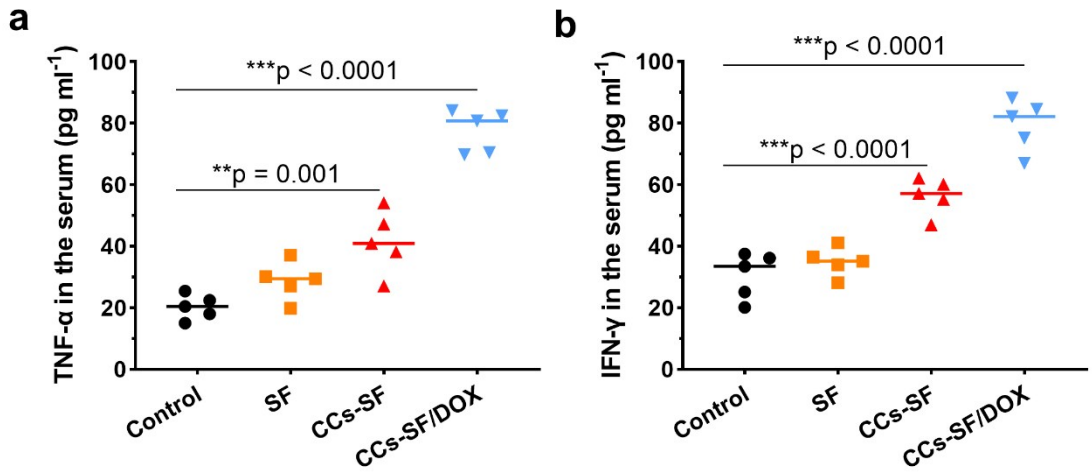

Figure S16. Cytokine levels of IFN-γ (a) and TNF-α (b) in the tumors. 4T1 tumors and serum were extracted from Balb/c mice 5 days after treatment. Data were expressed as the mean ± SD (n = 5, *P < 0.05; **P < 0.01; ***P < 0.001).

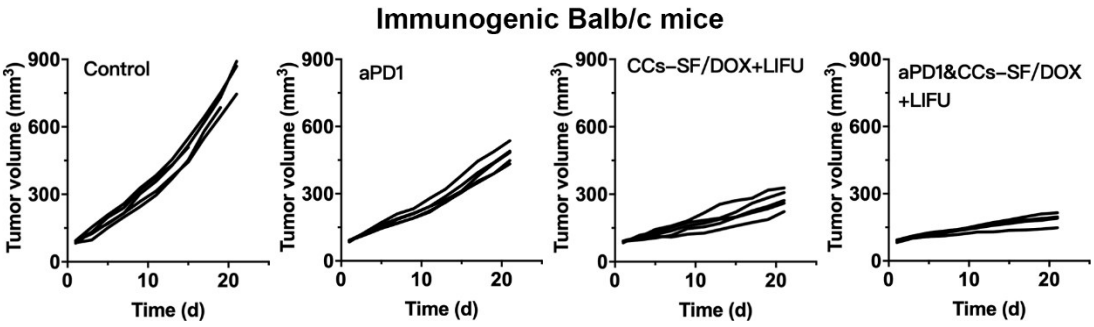

Figure S17. Individual tumor growth kinetics of different groups in immunogenic Balb/c mice.

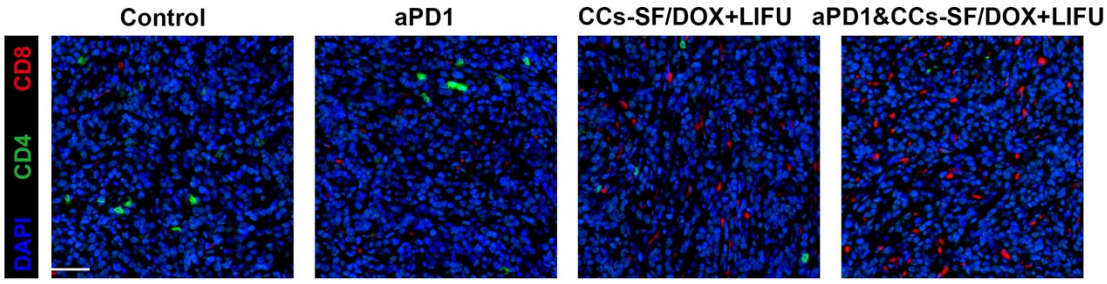

Figure S18. Immunofluorescence analysis of $CD4^+$ T cell and $CD8^+$ T cell infiltration in tumors with different treatments. Scale bars = 50 μm.